

1 **Assimilation of Freeze/Thaw Observations into the NASA Catchment Land Surface Model**

2
3 Leila Farhadi^{1,2}, Rolf H. Reichle¹, Gabriëlle J. M. De Lannoy^{1,3}, and John S. Kimball⁴

4
5 ¹Global Modeling and Assimilation Office, NASA Goddard Flight Center, Greenbelt, MD, USA

6 ²Department of Civil and Environmental Engineering, George Washington University,
7 Washington, DC, USA

8 ³Universities Space Research Association, NASA Goddard Space Flight Center, Greenbelt, MD,
9 USA

10 ⁴Flathead Lake Biological Station, Division of Biological Sciences, The University of Montana,
11 Polson, MT, USA

24 **Abstract**

25 The land surface freeze/thaw (F/T) state plays a key role in the hydrological and carbon
26 cycles and thus affects water and energy exchanges and vegetation productivity at the land
27 surface. In this study, we developed an F/T assimilation algorithm for the NASA Goddard Earth
28 Observing System, version 5 (GEOS-5) modeling and assimilation framework. The algorithm
29 includes a newly developed observation operator that diagnoses the landscape F/T state in the
30 GEOS-5 Catchment land surface model. The F/T analysis is a rule-based approach that adjusts
31 Catchment model state variables in response to binary F/T observations, while also considering
32 forecast and observation errors. A regional observing system simulation experiment was
33 conducted using synthetically generated F/T observations. The assimilation of perfect (error-free)
34 F/T observations reduced the root-mean-square errors (RMSE) of surface temperature and soil
35 temperature by 0.206 °C and 0.061 °C, respectively, when compared to model estimates
36 (equivalent to a relative RMSE reduction of 6.7% and 3.1%, respectively). For a maximum
37 classification error (CE_{max}) of 10% in the synthetic F/T observations, the F/T assimilation
38 reduced the RMSE of surface temperature and soil temperature by 0.178 °C and 0.036 °C,
39 respectively. For $CE_{max}=20\%$, the F/T assimilation still reduces the RMSE of model surface
40 temperature estimates by 0.149 °C but yields no improvement over the model soil temperature
41 estimates. The F/T assimilation scheme is being developed to exploit planned operational F/T
42 products from the NASA Soil Moisture Active Passive (SMAP) mission.

43

44 **1. Introduction**

45 Over one-third of the global land area undergoes a seasonal transition between
46 predominantly frozen and non-frozen conditions each year (Kim et al. 2011). This land surface
47 freeze/thaw (F/T) transition is closely linked to the timing and length of the vegetation growing
48 season (e.g. Black et al. 2000; Grippa et al. 2005; Kimball et al. 2006), the seasonal evolution of
49 land-atmosphere carbon dioxide exchange (Goulden et al. 1998) and the timing of seasonal
50 snowmelt, soil thaw and spring flood pulses (Kimball et al. 2001; Rawlins et al. 2005; Kane et al.
51 2008). The land surface F/T state thus acts as a natural on/off switch for hydrological and
52 biospheric processes over northern land areas and upper elevations where seasonal frozen
53 temperatures represent a significant portion of the annual cycle (Kim et al. 2011).

54 Studies show that the growing season, vegetation productivity and land-atmosphere CO₂
55 exchange patterns are shifting as a result of global warming (e.g. Randerson et al. 1999; Nemani
56 et al. 2003). For example, Smith et al. (2004), McDonald et al. (2004) and Kimball et al. (2006)
57 found consistency between these patterns and changes in seasonal F/T dynamics observed by
58 satellite microwave remote sensing. Thus, for more accurate modeling and prediction of land
59 surface hydrological and biospheric processes, a good representation of the landscape F/T state
60 in land surface schemes is needed. Recent efforts to enhance F/T modeling through improved
61 and more expansive representation of permafrost include work on the Community Land Model
62 (CLM; Lawrence et al. 2008; Lawrence et al. 2012), ORCHIDEE (Koven et al. 2009), the joint
63 UK Land Environment Simulator (JULES; Dankers et al. 2011) and the pan-Arctic Water
64 Balance Model (Rawlins et al. 2013)

65 Surface air temperature measurements from regional weather stations can provide an
66 indication of the landscape F/T state. However, the limited coverage of global weather station

67 networks, especially at higher latitudes and elevations, severely limits the capability for global
68 monitoring and the ability to capture F/T spatial and temporal patterns (Kim et al. 2011).
69 Satellite observations of passive and active microwaves are well suited for characterizing the
70 landscape F/T state (Frolking et al. 1999; Bateni et al. 2012; Kontu et al. 2010). Lower
71 frequency (≤ 37 GHz) microwave observations vary significantly between frozen and thawed
72 landscapes as a result of the strong sensitivity to contrasting dielectric properties. A number of
73 algorithms have been developed to detect the landscape F/T state at 25 – 50 km resolution using
74 brightness temperature measurements from the Advanced Microwave Scanning Radiometer for
75 the Earth Observing System (Zhao et al. 2011), the Scanning Multichannel Microwave
76 Radiometer (Zuerndorfer et al. 1992), the Special Sensor Microwave Imager (Zhang et al. 2001)
77 and the Soil Moisture and Ocean Salinity mission (Kontu et al. 2010). Similarly, radar
78 backscatter data have been utilized in several studies for the detection of the land surface F/T
79 state (Frolking et al. 1999; Kimball et al. 2001; Bartsch et al. 2011). The L-band (1.4 GHz) radar
80 observations from the Soil Moisture Active Passive (SMAP) mission (to be launched in 2014)
81 will provide a global classification of the F/T state at a 3 km spatial resolution and with a 3-day
82 temporal fidelity (Entekhabi et al. 2012).

83 The assimilation of remotely sensed F/T retrievals into land surface models might improve
84 the simulation of carbon and hydrological processes that are especially relevant during F/T
85 transitions. In this study the potential of the F/T assimilation to improve estimates of land
86 surface (skin) and soil temperature is investigated. To this end, an algorithm was developed for
87 the assimilation of binary F/T observations into the NASA Catchment land surface model
88 (Koster et al. 2000) within the NASA Goddard Earth Observing System, version 5 (GEOS-5)
89 modeling and assimilation framework. The assimilation algorithm includes a newly developed

90 observation operator that diagnoses the F/T state of the Catchment model and is compatible with
91 the information contained in the remotely sensed landscape F/T state at different microwave
92 frequencies. The F/T analysis consists of a rule-based approach that updates Catchment model
93 prognostic variables for surface and soil temperature in response to binary F/T observations and
94 considers forecast and observation errors. In order to test the methodology, an observing system
95 simulation experiment is conducted using synthetically generated F/T observations. The ultimate
96 goal of this study is to provide a framework for the assimilation of F/T retrievals from SMAP
97 into the Catchment model in the context of the SMAP Level 4 Surface and Root Zone Soil
98 Moisture (L4_SM) algorithm (Reichle et al. 2012) and the SMAP Level 4 Carbon algorithm
99 (Kimball et al. 2012). Future research will explore the direct assimilation of brightness
100 temperature or backscatter measurements to analyze the landscape F/T state.

101

102 **2. F/T detection using remote sensing**

103 At microwave frequencies, the landscape dielectric constant and thus the radar backscatter
104 and the emission of passive microwaves undergo large temporal changes associated with
105 corresponding changes in the predominant landscape F/T state within the satellite footprint
106 (Mironov et al. 2010), which makes space-borne microwave measurements well suited for global
107 F/T monitoring (Kim et al. 2011). In most studies, 0 °C is considered the temperature threshold
108 between the frozen and thawed states (Colliander et al. 2012). The temperature at which the F/T
109 transition occurs, however, varies with the water solute concentration and shows strong
110 heterogeneity across different landscape elements and within the satellite field of view. Thus, the
111 0 °C threshold is only an approximation of the landscape F/T transition point.

112 The contribution of different land surface elements to the retrieved F/T index depends on the
113 microwave frequency used for the F/T classification. Colliander et al. (2012) used QuickScat Ku
114 band (13.4 GHz) backscatter measurements to investigate the relationship between individual
115 land surface elements (e.g. soil, snow cover, and vegetation) and the aggregate landscape F/T
116 state indicated by the surface backscatter. It was observed that the temperature of the soil and
117 that of vegetation stems and branches are generally better indicators of Ku band F/T dynamics
118 than surface air temperature, with soil temperature being a better indicator than vegetation
119 temperature. Colliander et al. (2012) did not consider the effect of snow cover despite the fact
120 that for their study domain the frozen condition is dominated by a snow-covered landscape. The
121 rationale for their approach is the fact that the landscape thawing can be detected even under
122 snow-covered conditions, as demonstrated by Kimball et al. (2004a,b) using Ku-band
123 measurements from the NASA Scatterometer. Due to their longer wavelength, L-band (1.4 GHz)
124 observations from SMAP should be less sensitive to snow and vegetation scattering effects under
125 dry/frozen snow conditions and penetrate more deeply into the soil than Ku-band measurements.
126 This increases the sensitivity of the microwave signals to the F/T state of the underlying surface
127 soil layer.

128 However, for wet snow the penetration depth of microwaves is drastically reduced to a few
129 centimeters or less (Mätzler et al. 1984). Thus, sensitivity to soil conditions is minimal under wet
130 snow and the satellite signal will largely reflect snow cover conditions when a significant amount
131 of wet snow is present on the surface.

132

133

134

135 3. F/T diagnosis using the Catchment land surface model

136 This section first provides a brief description of the NASA GEOS-5 Catchment model
137 (Koster et al. 2000; Ducharne et al. 2000; Reichle et al. 2011; Reichle 2012), a state-of-the-art
138 global land surface model. Next, an observation operator is introduced for the diagnosis of the
139 landscape F/T state in the model. This observation operator is needed for the F/T analysis
140 (section 4) and designed to be compatible with the information contained in remotely sensed F/T
141 observations at different microwave frequencies.

142

143 *a. Catchment model overview*

144 The Catchment model's basic computational unit is the hydrological catchment (or
145 watershed). In each catchment, the vertical profile of soil moisture is determined by the
146 equilibrium soil moisture profile from the surface to the water table and by two additional
147 variables that describe deviations from the equilibrium profile in a 1-m root zone layer and in a
148 2-cm surface layer, respectively. Based on soil moisture, each catchment is separated into three
149 distinct and dynamically varying subareas: a saturated region, an unsaturated region and a
150 wilting region. The Catchment model also includes a three-layer snow model that accounts for
151 snow melting and refreezing, dynamic changes in snow density, snow insulating properties, and
152 other physics relevant to the growth and ablation of the snowpack (Stieglitz 1994).

153 In the snow-free portion of the catchment, the surface energy balance is computed separately
154 for the saturated, unsaturated, and wilting subareas of each catchment. In each of these three
155 subareas, the land surface temperature is modeled with surface temperature prognostic variables
156 that are specific to the soil moisture regime (T_{C1} for the saturated region, T_{C2} the for unsaturated
157 region and T_{C4} for wilting region). For tropical forest land tiles, the T_{C1} , T_{C2} and T_{C4} fields are tied

158 to approximately the top 5 cm of soil, whereas for all other tiles the effective soil depth associated
159 with these variables is negligible (Reichle 2012). The area-weighted average of the three
160 prognostic surface temperature variables determines the surface temperature in the absence of
161 snow, $T_{surf}^{no-snow}$, which is then averaged (again area-weighted) with the surface snow temperature,
162 T_{surf}^{snow} , to provide the land surface temperature T_{surf} of the entire catchment:

163

$$164 \quad T_{surf} = (1 - asnow)T_{surf}^{no-snow} + (asnow)T_{surf}^{snow} \quad (1)$$

165

166 The surface snow temperature and the snow area fraction (*asnow*) are themselves diagnosed
167 from the model's snow prognostic variables (snow water equivalent, snow depth, and snow heat
168 content).

169 Subsurface temperatures are modeled using a soil heat diffusion model that consists of six
170 layers. The thicknesses of the layers are about 10, 20, 40, 75, 150, and 1,000 cm starting from the
171 top-most soil temperature layer. The layer thicknesses are the same for all land tiles. (For
172 tropical forests, the layers of the heat diffusion model are shifted downward by the 5 cm
173 thickness of the surface layer; see above.) The prognostic variables for the heat diffusion model
174 are the ground heat contents (*ght*) in the six layers from which the soil temperatures (T_{soil}) in
175 each layer are diagnosed. For the remainder of this paper, *ght* and T_{soil} refer to the values in the
176 top-most (10 cm thick) soil layer only.

177

178 *b. Freeze/thaw state in the Catchment model*

179 The F/T analysis (section 4) requires diagnosing the landscape F/T state of the Catchment
180 model based on its prognostic variables. As outlined in section 2, the landscape F/T state
181 observed by L-band microwave remote sensing is assumed to be primarily related to the near-
182 surface soil and vegetation canopy temperature under dry/frozen snow condition. Under wet
183 snow, however, the satellite F/T signal will largely reflect snow cover conditions. We therefore
184 first define an effective temperature that vertically averages the (snow-free) portion of the
185 surface temperature, $T_{surf}^{no-snow}$, and the top-layer soil temperature T_{soil} .

186

$$187 \quad T_{eff} = (1 - \alpha)T_{soil} + \alpha T_{surf}^{no-snow} \quad (2)$$

188

189 Given the wavelengths used for F/T remote sensing, which typically range from 1 cm to 20 cm,
190 and the resulting penetration depths, the contribution of the lower-layer soil temperatures to the
191 microwave signal is small and neglected here. The parameter α determines the relative
192 contributions of the surface temperature and the soil temperature and can be adjusted according
193 to the microwave frequency used for the F/T classification so that it better reflects sensor signal
194 penetration depth. Besides the (snow-free) effective temperature, T_{eff} , additional information on
195 the landscape F/T state is contained in the modeled snow conditions. Here, the snow cover area
196 fraction, $asnow$, is most relevant. In the Catchment model, the snow cover fraction increases
197 linearly with the snow water equivalent (SWE) during the accumulation phase and reaches full
198 cover ($asnow=100\%$) when the total amount of SWE accumulated over the catchment reaches a
199 model constant of $WEMIN=26 \text{ kg m}^{-2}$ (Reichle et al., 2011).

200 The landscape F/T state is then diagnosed from the Catchment model variables via the
201 following observation operator, which is also illustrated in Figure 1:

202

203 Thawed (F/T=1) *if* $T_{eff} \geq T_{eff-Threshold}$ *and* $asnow < asnow_{Threshold}$
204 (3)

205 Frozen (F/T=-1) *if* $T_{eff} < T_{eff-Threshold}$ *or* $asnow \geq asnow_{Threshold}$
206

207 The effective temperature that determines the transition between frozen and thawed
208 conditions is $T_{eff-Threshold} = 0^{\circ}C$. The snow cover threshold value $asnow_{Threshold}$ determines the
209 maximum modeled snow cover fraction that is still compatible with a thawed condition. This
210 value is fixed at 10% in this study and depends on the microwave frequency and the associated
211 penetration depth through snow. The penetration depth at C-band (5.6 GHz) can be as large as
212 several meters in dry snow conditions (Bingham and Drinkwater 2000, Dall et al. 2001) and is
213 likely even larger at L-band (1.27 GHz; Rignot et al. 2001). For wet snow, however, the
214 penetration depth of microwaves is drastically reduced to a few centimeters or less (Mätzler et al.,
215 1984).

216

217 **4. F/T data assimilation module (F/T analysis)**

218 The assimilation of F/T observations is conceptually similar to the assimilation of snow
219 cover observations. In both cases, the observed variable is, at least at a finer spatial scale,
220 essentially a binary observation. Binary observations cannot be assimilated with a Kalman filter,
221 because this requires continuous variables. For the assimilation of F/T observations, we propose
222 a rule-based assimilation approach, similar to the rule-based assimilation of binary snow cover
223 observations (Rodell and Houser 2004). In short, if the model forecast and the corresponding
224 SMAP observations disagree on the F/T state, that is, if the model indicates frozen conditions
225 and observation indicates thawed conditions (or vice versa), the model prognostic variables

226 related to the soil temperature (T_{soil}) and the snow-free surface temperature ($T_{surf}^{no-snow}$) are
 227 adjusted to match the observed F/T condition more closely. To account for model and
 228 observation errors, the delineation between frozen and thawed regimes is defined with some
 229 uncertainty in the assimilation algorithm, as will be detailed below.

230

231 *a. Uncertainty in F/T simulations and observations*

232 The perhaps simplest F/T analysis could use the observation operator defined in Equation (3)
 233 to determine the F/T state of the model forecast and then apply increments to switch the model's
 234 F/T state whenever the model's F/T state differs from that of the observations. However, such an
 235 analysis would ignore any uncertainty associated with the formulation of the observation
 236 operator (Equation (3)). It would also ignore any errors in the observations themselves.

237 For the purpose of the F/T analysis, we therefore refine the observation operator by
 238 introducing a regime of undetermined F/T status, which is defined by upper and lower bounds
 239 for the effective temperature and snow cover thresholds, as illustrated in Figure 2. Specifically,
 240 the model F/T state for the purpose of the F/T analysis is:

241

$$\begin{aligned}
 242 \quad & \text{Completely Thawed (F/T=1)} && \text{if } T_{eff} > UB_{T_{eff}} \text{ and } asnow < LB_{asnow} \\
 243 \quad & \text{Completely Frozen (F/T=-1)} && \text{if } T_{eff} < LB_{T_{eff}} \text{ or } asnow > UB_{asnow} \quad (4) \\
 244 \quad & \text{Undetermined (F/T=0)} && \text{otherwise}
 \end{aligned}$$

245

246 In this study, $UB_{T_{eff}}$ and $LB_{T_{eff}}$ are fixed at -1°C and $+1^{\circ}\text{C}$, and LB_{asnow} is set to 5%. A
 247 value of 100% was chosen for UB_{asnow} . This assigns an “undetermined” F/T regime to
 248 situations with considerable snow cover on soil that is thawed or close to thawing. Under these

249 circumstances, it is difficult to determine whether the model F/T state should be thawed or frozen
250 in a manner that would be fully consistent with the retrieval algorithm that was used to determine
251 the value of the F/T observation.

252 The “undetermined” regime impacts the computation of the increments in two ways. Firstly,
253 if the model forecast F/T state is “undetermined”, no increments will be applied. Secondly, the
254 upper and lower bounds for the effective temperature threshold ($UB_{T_{eff}}$, $LB_{T_{eff}}$) will be used to
255 formulate the rule-based increments that result from the F/T analysis (section 4b). In either case,
256 the “undetermined” regime implicitly assigns weight to the model forecast in the analysis update
257 and thus assumes imperfect observations.

258

259 *b. Update rules*

260 The assimilation of F/T observations is based on a number of rules. No updates are
261 performed (i) if both the model and the observations agree on the F/T state, or (ii) if the model
262 F/T state is undetermined per Equation (4). When the observations and simulations indicate a
263 contrasting F/T state, then the model prognostic variables associated with T_{eff} are updated (i.e.,
264 T_{C1} , T_{C2} , T_{C4} , and ght ; section 3). Specifically, if the observations indicate a thawed condition
265 (F/T=1) whereas the model is in a frozen regime, then T_{eff} is increased to the lower bound
266 $LB_{T_{eff}}$. Conversely, if the observations indicate freezing (F/T=-1) and the model is in a thawed
267 regime, then T_{eff} is decreased to the upper bound $UB_{T_{eff}}$. The updates can be summarized as
268 follows:

269

270 If obs F/T=-1, model F/T=1 and $\Delta T = (UB_{T_{eff}} - T_{eff}^-) < 0$, then $T_{eff}^+ = T_{eff}^- + \Delta T$
271

272 If obs F/T=1, model F/T=-1 and $\Delta T = (LB_{T_{eff}} - T_{eff}^-) > 0$, then $T_{eff}^+ = T_{eff}^- + \Delta T$
273

(5)

274 In this equation, T_{eff}^- represents the a priori estimate and T_{eff}^+ represents the analysis. The
275 same increment ΔT is applied to the prognostic temperature variables T_{C1} , T_{C2} and T_{C4} (the
276 weighted average of which determines $T_{surf}^{no-snow}$) and the soil temperature, T_{soil} . For the latter, the
277 ground heat content (ght , the model prognostic variable that determines the soil temperature) is
278 adjusted accordingly to match the updated soil temperature, T_{soil}^+ . Note that the updates to T_{C1} , T_{C2}
279 and T_{C4} also adjust T_{surf} following Equation (1). In this study we are only updating the surface
280 temperature and the soil temperature (and ground heat content) of the top-most soil layer. For
281 future studies, updating the temperature of lower soil layers can also be considered.

282 The update rules (Equation (5)) intentionally do not adjust the snow variables directly. As
283 mentioned in section 4a, an upper bound of $UB_{asnow}=100\%$ has been selected to avoid
284 uncertainties related to the role of snow in determining the F/T state. This choice is supported by
285 several experiments that were performed with smaller threshold values for UB_{asnow} and in
286 which a portion of the snow was removed if the observed F/T state indicated thawed conditions.
287 These additional experiments (not shown) indicated that (error-prone) F/T observations
288 sometimes mistakenly removed the model snow, which resulted in large subsequent forecast
289 errors. It is difficult to recover from such errors, because once the model snow has been
290 removed, the missing snow cannot easily be re-deposited at future analysis times due to the lack
291 of quantitative information about snow mass in the F/T observations. Consequently, in the
292 following the snow prognostic variables are not adjusted as part of the F/T analysis update.
293 Nevertheless, at later time steps the model's snow conditions will respond to the adjusted soil
294 temperatures and corresponding updated hydrological fluxes.

295

296

297

298 **5. Synthetic twin experiment**

299 The twin experiment consists of several components. A Catchment land surface model
300 integration serves as the “truth” and is used (i) to generate synthetic F/T observations and (ii) to
301 validate the analysis results. The data assimilation experiment is performed with imperfect
302 simulations and observations. The synthetic observed F/T state is obtained by adding
303 classification error to the true F/T state (Section 5b). The imperfect Catchment land surface
304 model integration is produced with a different forcing dataset to mimic forcing errors. This
305 imperfect model simulation without data assimilation is referred to as the open loop (OL) (see
306 discussion in section 5b). The F/T analysis is performed by assimilating the synthetic F/T
307 observations into the imperfect model simulation using erroneous forcing data, and is referred to
308 as the data assimilation (DA) integration. The OL and DA results are compared against the truth
309 and the relative importance of assimilating observed F/T data is investigated (section 6).

310

311 *a. Study domain and time period*

312 The study domain is a region in North America between 45-55°N and 90-110°W (Figure 3).
313 The simulations are performed on a 36 km Equal-Area Scalable Earth (EASE) grid, covering
314 1,137 grid cells in the study domain. The Catchment model integration is conducted using the
315 GEOS-5 land data assimilation system (Reichle et al. 2014) with a time step of 20 min. The
316 selected period of investigation is 8 years (1 January 2002 - 1 January 2010) and the temporal
317 resolution of the model output is 3-hourly. The model was spun up by cycling ten times through
318 the 1-year period from 1 January 2001 to 1 January 2002.

319

320

321 *b. Synthetic truth, synthetic observations, and open loop*

322 The synthetic truth is based on a Catchment model simulation that uses surface
323 meteorological forcing data from the Modern-Era Retrospective analysis for Research and
324 Applications (MERRA; Rienecker et al. 2011). The MERRA data product is provided at an
325 hourly temporal resolution and a $1/2^\circ \times 2/3^\circ$ (latitude/longitude) spatial resolution. The resulting
326 8 years of synthetic true hydrological state variables and fluxes are used for the validation of the
327 F/T analysis (DA). The synthetic true F/T state is obtained by applying the observation operator
328 (Equation (3)) using $\alpha = 0.5$, $asnow_{Threshold} = 10\%$, and $T_{eff-Threshold} = 0^\circ C$.

329 The synthetic observed F/T indices are obtained by corrupting the true F/T data set with
330 synthetic classification error. Specifically, the classification error is defined by the probability of
331 misclassification. The SMAP mission requirements call for a F/T product with no more than
332 20% mean spatial classification error (McDonald et al. 2012). Here, we assume that the
333 classification error is greatest near $0^\circ C$, where it reaches CE_{max} , linearly tapers off towards
334 colder and warmer temperatures and vanishes below $-10^\circ C$ and above $+10^\circ C$. That is, the
335 classification error is given by a piecewise linear function of the land surface temperature, T_{surf} ,
336 as follows:

$$337 \left\{ \begin{array}{ll} CE_{max} \frac{T_{surf} + 10}{10} & -10^\circ C \leq T_{surf} \leq 0^\circ C \\ CE_{max} \frac{10 - T_{surf}}{10} & 0^\circ C \leq T_{surf} \leq 10^\circ C \\ 0 & T_{surf} > 10^\circ C \text{ or } T_{surf} < -10^\circ C \end{array} \right. \quad (6)$$

338 This parameterization of the classification error is illustrated in Figure 4.

339 The synthetic F/T observations are generated at each time and for each location (or grid cell)
340 by obtaining the probability of misclassification based on the land surface temperature T_{surf} from
341 Equation (6). We then randomly select a number from a uniform distribution between 0 and 1. If
342 the selected random number is less than the specified classification error for that land surface
343 temperature, then the observed F/T index is obtained by changing the sign of true F/T
344 classification. Otherwise, the observed F/T index is equal to the true F/T state. The sensitivity of
345 the data assimilation experiments to different levels of observation classification errors will be
346 investigated below.

347 The open loop data set is obtained from an integration of the Catchment model with forcing
348 data that differ from those used for the truth. Forcing errors were imposed by replacing the
349 MERRA surface meteorological forcing fields with data from the Global Land Data Assimilation
350 System (GLDAS; Rodell et al. 2004) as used in a former version of the NASA GMAO seasonal
351 prediction system at 3-hourly temporal resolution and at $2.0^{\circ} \times 2.5^{\circ}$ (latitude/longitude) spatial
352 resolution. The hydrological response associated with the differences between MERRA and
353 GLDAS in precipitation and radiation timing and intensity results in considerable differences in
354 the diagnosed F/T state at the grid scale.

355 *c. F/T assimilation setup*

356 The F/T assimilation experiment uses the same model settings as described for the open loop
357 model, that is, it uses GLDAS forcings to mimic forcing errors relative to the MERRA truth. No
358 additional perturbations are imposed and a single deterministic integration is performed for a
359 period of 8 years (1 January 2002 – 1 January 2010). In this study, the synthetic observed F/T
360 index is assimilated into the imperfect model integration at 6:00am and 6:00pm local time (F/T

361 analysis update). The proposed assimilation time steps are compatible with the planned overpass
362 times of SMAP.

363 The various tunable parameters in the diagnosis of the (uncertain) F/T state and the update rules
364 are as follows. The parameter α (which determines the weight of the components of the
365 effective temperature, Equation (2)) is set to 0.5 for the generation of F/T observations. This
366 parameter is tunable and the sensitivity of data assimilation experiments to this parameter in the
367 observation operator (Equation (3)) will be explored in section 6b. The values for the lower and
368 upper bounds on the snow cover threshold [LB_{asnow} ; UB_{asnow}] are 5% and 100% snow
369 cover, respectively. The uncertainty range for $asnow$ accounts for the combined uncertainty
370 associated with the diagnosis of the modeled F/T state and the classification of the F/T
371 observations in the presence of snow. In order to account for the uncertainty of the 0°C threshold
372 value resulting from water solute concentration across different landscape elements within the
373 satellite field of view, the upper and lower bounds for the effective temperature thresholds are
374 +1°C and -1°C, respectively. The F/T analysis may benefit from adjusting these uncertainty
375 bounds in response to the F/T classification error in the synthetic observations, but in the present
376 paper we keep the bounds fixed.

377

378 *d. Validation of temperature estimates*

379 By design, the analysis update (Equation (5)) does not alter the F/T state of the model
380 forecast, but the update rules will alter the temperature variables whenever the model forecast
381 F/T state differs from the observed F/T index. It is expected that the differences in surface and
382 soil temperatures (with respect to the truth) are smaller in the assimilation estimates than in the

383 open loop estimates. We therefore focus the validation on the computation of root-mean-square
384 errors (RMSE) of surface and soil temperatures versus the truth data set.

385 F/T data assimilation is expected to be most relevant when temperatures are near 0°C
386 because it is straightforward to estimate the F/T state accurately during clearly warm or cold
387 conditions. We thus limit the validation to time steps where the air temperature is above -7°C
388 and below +7°C (as indicated by the MERRA surface air temperatures). Furthermore, we restrict
389 the validation to 6:00 am and 6:00 pm local time only, compatible with the time of the SMAP
390 overpasses.

391

392 **6. Results and discussion**

393 *a. Open loop (OL) and data assimilation (DA) with standard settings*

394 To assess the impact of the imperfect forcing on the diagnosis of the F/T state without data
395 assimilation, we first examine the OL results. As mentioned in section 5, the OL utilizes GLDAS
396 forcings and the “truth” utilizes MERRA forcings. When compared to the truth, the OL has a
397 F/T classification error of 4.85% (Table 1). The table also shows that the RMSE value for the
398 OL surface temperature (T_{surf}) is 3.1°C and that of the first soil layer temperature (T_{soil}) is 2.0°C.

399 Again, by design the F/T analysis update does not alter the F/T state of the model forecast,
400 and consequently the F/T classification error of the assimilation estimates is the same as that of
401 the OL. But through the assimilation of the F/T observations, we hope to reduce the OL
402 temperature errors. The F/T analysis involves adjusting the land surface effective temperature
403 (T_{eff}), and subsequently $T_{surf}^{no-snow}$ and T_{soil} , if the observed and simulated F/T states do not agree.
404 Table 2 summarizes the reduction in RMSE ($\Delta RMSE = RMSE_{OL} - RMSE_{DA}$) by

405 assimilating synthetic F/T observations with 4 different levels of classification error (CE_{max}), and
406 assuming default values for the tunable parameters, as introduced in section 5c.

407 Assimilating observed F/T indices without classification error results in an RMSE
408 improvement of 0.206°C for the land surface temperature (T_{surf}) and an RMSE improvement of
409 0.061°C for the first layer soil temperature. When compared to the OL results for these two
410 variables, the F/T analysis results in relative RMSE improvements of 6.7% and 3.1% for T_{surf}
411 and T_{soil} , respectively. The skill improvement decreases monotonically with increasing
412 classification error in the observations. For a maximum classification error of $CE_{max}=20\%$ the
413 assimilation of F/T observations still reduces the surface temperature RMSE by 0.149°C but it no
414 longer improves the soil temperature estimates.

415 Figure 5 shows the T_{surf} and T_{soil} skill improvements in the study domain for the assimilation
416 of F/T observations with $CE_{max}=0\%$, 5% and 20%. Figures 5a and 5b show that as a result of
417 assimilating perfect F/T observations, the skill of T_{surf} and T_{soil} improves for almost all grid cells
418 within the study domain. However, the efficiency of the F/T analysis deteriorates as the
419 classification error is increased (Figures 5c-d). For $CE_{max}=20\%$, many grid cells in the study
420 domain have negative or no improvement in T_{soil} skill. As mentioned above, the F/T analysis
421 may benefit from adjusting the uncertainty bounds in response to the classification error of the
422 synthetic F/T observations, but the above results indicate that using a single set of uncertainty
423 bounds already provides reasonable assimilation estimates.

424 Figure 6 shows the skill improvement for each grid cell binned as function of the number of
425 analysis updates per grid cell (that is, the skill improvement is spatially averaged across grid cells
426 experiencing a similar number of analysis updates in time within the study domain). The data

427 points are assigned to 6 bins with equal numbers of grid cells. Each bin center is assigned the
428 average number of analysis updates for the grid cells in that particular bin. When more error-
429 free observations (Figure 6a,b) or observations with modest classification errors (Figure 6c,d) are
430 assimilated, the average skill improves with the number of analysis updates for both the
431 temperatures, T_{surf} and T_{soil} . However, as the maximum classification error is increased to 20%
432 (Fig 6e,f), the average skill in the temperature variables does not improve with the number of
433 analyses. This is due to the negative effect of assimilating misclassified observed F/T indices
434 into the model.

435

436 *b. Sensitivity of assimilation results to the formulation of the effective temperature*

437 The effective temperature, T_{eff} , which is an important variable in diagnosing the F/T state, is
438 a weighted average of the surface temperature in the absence of snow, $T_{surf}^{no-snow}$, and the soil
439 temperature, T_{soil} (Equation (2)). The weight (α) should be a function of the microwave
440 penetration depth. An increase (decrease) in penetration depth results in a decrease (increase) in
441 parameter α and hence an increase (decrease) in the weight of the soil temperature component of
442 effective temperature T_{eff} . In this study, the synthetic true F/T state was obtained based on the
443 assumption that the parameter α equals 0.5. Thus, $T_{surf}^{no-snow}$, and T_{soil} have similar weights in
444 determining the effective temperature, T_{eff} , and thus the F/T state of the soil.

445 However, when determining the F/T index from (real) remote sensing observations, the
446 relative effect of $T_{surf}^{no-snow}$ and T_{soil} in those observations is not known a priori. Here we investigate
447 the sensitivity of the DA performance to the choice of this factor in the observation operator. A

448 physically meaningful range of α between 0.25 and 1 was selected. This means that the weight
449 of soil temperature, T_{soil} , ranges between 0.75 and 0 in the model.

450 The sensitivity of the assimilation results to the value of α in the forecasted F/T state is
451 illustrated Figure 7. The skill improvements ($\Delta RMSE$) are shown for the case where no
452 classification error ($CE_{max}=0\%$) is associated with the assimilated F/T indices. As expected, the
453 maximum skill improvement for both T_{surf} and T_{soil} occurs when the parameter α is 0.5, that is,
454 when the α value that is used in the observation operator of the assimilation system matches the
455 α value that was used to generate the synthetic F/T observations. The figure shows that the
456 sensitivity of T_{surf} to the parameter α seems to be higher than that of T_{soil} . The skill of T_{surf} is
457 reduced by up to 50% when α is not selected correctly, while the skill is reduced by at most 8%
458 for T_{soil} . It is thus important to understand how different land surface variables contribute to the
459 observed F/T and to mimic this relationship adequately in the F/T observation operator used in
460 the data assimilation scheme.

461

462 7. Conclusions

463 In this study an algorithm for the diagnosis of the F/T state in the NASA Catchment land
464 surface model was developed. The algorithm is compatible with the information contained in
465 remotely sensed retrievals of landscape F/T state at different microwave frequencies. The GEOS-
466 5 land data assimilation system in offline mode was updated with the newly designed F/T
467 assimilation module. The ultimate goal of this research is to provide a framework for the
468 assimilation of SMAP (Soil Moisture Active Passive) F/T observations into the Catchment
469 model.

470 The performance of the method for a synthetic experiment showed encouraging
471 improvements in the skill of soil temperature and land surface temperature estimates. However,
472 the average skill improvement depends on the classification error in the F/T observations. In our
473 synthetic study, the open loop simulation has a modeled F/T classification error of 4.85% error
474 compared to the truth. When assimilating perfect (error-free) F/T observations, the RMSE for
475 land surface temperature (T_{surf}) and soil temperature (T_{soil}) improves by 6.7% and 3.1%,
476 respectively. Yet, the skill improvement decreases monotonically with increasing classification
477 error in the assimilated F/T observations. No more improvements in soil temperature were found
478 with maximum classification errors of $CE_{max}=20\%$.

479 The results also discuss the sensitivity of the data assimilation (DA) to the α parameter in the
480 observation operator. This parameter controls the relative contribution of the snow-free surface
481 temperature and the top-layer soil temperature to the F/T state in the modeling system and
482 impacts the temperature increments applied during the F/T analysis. The maximum skill
483 improvement can only be expected if the observation operator in the modeling system closely
484 mimics the relative importance of various landscape components, including the surface and soil
485 temperatures, in the determination of the satellite F/T observations. Therefore, the observation
486 operator could also benefit from further tuning to improve the linkage between the modeled
487 snow cover and the expected F/T index retrieved from the microwave signal. Moreover, the
488 limitations of the present study could perhaps be overcome in the future by directly assimilating
489 backscatter or brightness temperature observations (instead of F/T retrievals).

490 The regional domain of the experiment investigated in this research represents a relatively
491 flat terrain area of central North America. In this region, the model without assimilation (open
492 loop) produced a F/T classification error of only 4.85%. This modeling error is a direct result of

493 the assumption that all F/T classification errors are solely due to errors in the forcing data (as
494 reflected in the difference between the GLDAS and MERRA data). When the F/T assimilation
495 method is applied to satellite observations (instead of synthetic retrievals), we expect larger
496 errors in the simulated F/T state, especially over regions with more complex topography (e.g.,
497 regions in Western North America) where global forcing fields do not resolve the considerable
498 heterogeneity of the surface conditions. In applications, the benefit of assimilating high-
499 resolution (3 km) SMAP F/T retrievals is therefore expected to be greater for improving the
500 simulation of eco-hydrological processes.

501

502 **Acknowledgments**

503 This study was funded through support from the SMAP Science Definition team and the NASA
504 program on the Science of Terra and Aqua.

505

506

507

508 **References**

509 Bartsch, A., Sabel, D., Wagner, W., and S.E., 2011: Considerations for derivation and use of soil
510 moisture data from active microwave satellites at high latitudes. *In Geoscience and Remote*
511 *Sensing Symposium (IGARSS), Vancouver, Canada, IEEE International, 3132-3135*

512

513 Bateni, S.M., Huang, C., Margulis, S.A., Podest, E., McDonald, K., 2013: Feasibility of
514 characterizing snowpack and the freeze-thaw state of underlying soil using multifrequency
515 active/passive microwave data. *IEEE Trans Geosci Remote Sens.*, **51**,1-18

516

517 Betts, A. K., Ball, J. H., McCaughey, J. H., 2001: Near-surface climate in the boreal
518 forest. *Journal of Geophysical Research*, **106**(D24), 33529-33.

519

520 Bingham, A. W., Drinkwater, M. R., 2000: Recent changes in the microwave scattering
521 properties of the Antarctic ice sheet. *IEEE Trans Geosci Remote Sens.*, **38**(4), 1810-1820.

522

523 Black, T. A., Chen, W. J., Barr, A. G., Arain, M. A., Chen, Z., Nesic, Z., Hogg, E. H., Neumann,
524 H. H., Yang, P. C., 2000 :Increased carbon sequestration by a boreal deciduous forest in years
525 with a warm spring. *Geophysical Research Letters*, **27**(9), 1271-1274

526

527 Colliander, A., McDonald, K., Zimmermann, R., Schroeder, R., Kimball, J. S., Njoku, E. G.,
528 2012: Application of QuikSCAT Backscatter to SMAP Validation Planning: Freeze/Thaw State

529 Over ALECTRA Sites in Alaska From 2000 to 2007. *IEEE Trans Geosci Remote Sens.*, **50**(2),
530 461-468.
531

532 Dall, J., Madsen, S. N., Keller, K., Forsberg, R., 2001: Topography and penetration of the
533 Greenland ice sheet measured with airborne SAR interferometry. *Geophysical Research Letters*,
534 **28**(9), 1703-1706.
535

536 Dankers, R., Burke, E. J., Price, J., 2011: Simulation of permafrost and seasonal thaw depth in
537 the JULES land surface scheme. *The Cryosphere Discussions* **5**(2), 1263-1309.
538

539 Ducharne, A., Koster, R. D., Suarez, M. J., Stieglitz, M., Kumar, P., 2000: A catchment-based
540 approach to modeling land surface processes in a general circulation model 2. Parameter
541 estimation and model demonstration. *Journal of geophysical research*, **105**(D20), 24823-24.
542

543 Entekhabi, D., Njoku, E. G., O'Neill, P. E., Kellogg, K. H., Crow, W. T., Edelstein, W. N., ... &
544 Van Zyl, J., 2010). The soil moisture active passive (SMAP) mission. *Proceedings of the IEEE*,
545 **98**(5), 704-716.
546

547 Frohking, S., McDonald, K., Kimball, J., Zimmermann, R., Way, J. B, Running, S. W., 1999:
548 Using the space-borne NASA Scatterometer (NSCAT) to determine the frozen and thawed
549 seasons of a boreal landscape, *J. Geophys. Res.* **104**, 27895-27908.
550

551 Gouliden, M. L., Munger, J. W., FAN, S. M., Daube, B. C., Wofsy, S. C., 1996: Measurements of
552 carbon sequestration by long- term eddy covariance: Methods and a critical evaluation of
553 accuracy. *Global change biology*, **2**(3), 169-182.

554 Grippa, M., L. Kergoat, T. Le Toan, N. M. Mognard, N. Delbart, J. L'Hermitte, Vicente-Serrano,
555 S. M., 2005: The impact of snow depth and snowmelt on the vegetation variability over central
556 Siberia. *Geophysical Research Letters* **32** (21), L21412.

557

558 Kane, D.L., Hinzman, L.D., Gieck, R.E., McNamara, J. P., Youcha, E., Oatley, J. A., 2008:
559 Contrasting Extreme Runoff Events in Areas of Continuous Permafrost, Arctic Alaska.
560 *Hydrology Research*, **38**(4), 287-298

561

562 Kim, Y., Kimball, J. S., Zhang, K., McDonald, K. C., 2012: Satellite detection of increasing
563 Northern Hemisphere non-frozen seasons from 1979 to 2008: Implications for regional
564 vegetation growth. *Remote Sensing of Environment*, **121**, 472-487

565

566 Kim, Y., Kimball, J. S., McDonald, K. C., Glassy, J., 2011: Developing a global data record of
567 daily landscape freeze/thaw status using satellite passive microwave remote sensing. *IEEE Trans*
568 *Geosci Remote Sens.*, 49(3), 949-960.

569

570 Kimball, J. S., McDonald, K. C., Zhao, M., 2006: Spring thaw and its effect on terrestrial
571 vegetation productivity in the western Arctic observed from satellite microwave and optical
572 remote sensing. *Earth Interactions*, **10**(21), 1-22.

573

574 Kimball, J. S., McDonald, K. C., Keyser, A. R., Frohking, S., Running, S. W., 2001: Application
575 of the NASA Scatterometer (NSCAT) for determining the daily frozen and nonfrozen landscape
576 of Alaska. *Remote Sensing of Environment*, **75**(1), 113-126.

577 Kimball, J. S., McDonald, K. C., Frohking, S., Running, S. W., 2004a: Radar remote sensing of
578 the spring thaw transition across a boreal landscape. *Remote Sensing of Environment*, **89**(2), 163-
579 175.

580

581 Kimball, J. S., McDonald, K. C., Running, S. W., Frohking, S. E., 2004b: Satellite radar remote
582 sensing of seasonal growing seasons for boreal and subalpine evergreen forests. *Remote Sensing*
583 *of Environment*, **90**(2), 243-258.

584

585 Kimball, J. S., Reichle, R., O'Neill, P., McDonald, K., Njoku, E., 2012: SMAP Level 4 Carbon
586 Data Product (L4_C).

587

588 Kontu, A., Lemmetyinen, J., Pulliainen, J., Rautiainen, K., Kainulainen, J., Seppänen, J., 2010:
589 L-band measurements of boreal soil. *In Geoscience and Remote Sensing Symposium (IGARSS)*,
590 Honolulu, Hawaii, IEEE International, 706-709

591

592 Koster, R. D., Suarez, M. J., Ducharme, A., Stieglitz, M., Kumar, P., 2000: A catchment- based
593 approach to modeling land surface processes in a general circulation model: 1. Model
594 structure. *Journal of Geophysical Research: Atmospheres* (1984–2012), **105**(D20), 24809-
595 24822.

596

597 Koven, C., Friedlingstein, P., Ciais, P., Khvorostyanov, D., Krinner, G., Tarnocai, C., 2009: On
598 the formation of high-latitude soil carbon stocks: Effects of cryoturbation and insulation by
599 organic matter in a land surface model. *Geophysical Research Letters*, **36**(21), L21501.
600

601 Lawrence, D. M., Slater, A. G., Romanovsky, V. E., Nicolsky, D. J., 2008. Sensitivity of a model
602 projection of near-surface permafrost degradation to soil column depth and representation of soil
603 organic matter. *Journal of Geophysical Research*, **113**(F2), F02011.
604

605 Lawrence, D. M., Oleson, K. W., Flanner, M. G., Fletcher, C. G., Lawrence, P. J., Levis, S.,
606 Swenson, S. C., Bonan, G. B., 2012: The CCSM4 land simulation, 1850-2005: Assessment of
607 surface climate and new capabilities. *Journal of Climate* **25** (7),2240-2260.
608

609 Lynch-Stieglitz, M., 1994: The development and validation of a simple snow model for the GISS
610 GCM. *Journal of Climate*, **7**(12), 1842-1855.
611

612 Mätzler, C., and E. Schanda, 1984: Snow mapping with active microwave sensors. *Remote*
613 *Sensing* **5**(2), 409-422.
614

615 McDonald, K., Podest, E., Dunbar, S., Njoku, E., Kimball, J., 2012: SMAP Level 3 Radar
616 Freeze/Thaw Data Product.
617

618 McDonald, K. C., Kimball, J. S., Njoku, E., Zimmermann, R., Zhao, M., 2004: Variability in
619 springtime thaw in the terrestrial high latitudes: Monitoring a major control on the biospheric

620 assimilation of atmospheric CO₂ with spaceborne microwave remote sensing. *Earth*
621 *Interactions*, **8**(20),1-23.

622

623 Mironov, V. L., De Roo, R. D., Savin, I. V., 2010: Temperature-dependable microwave
624 dielectric model for an arctic soil. *IEEE Trans Geosci Remote Sens.*, **48**(6), 2544-2556.

625

626 Nemani, R.R., Keeling, C. D., Hashimoto, H., Jolly, W. M., Piper, S. C., Tucker, C. J., Myneni,
627 R. B., Running, S. W., 2003: Climate-driven increases in global terrestrial net primary
628 production from 1982 to 1999. *Science* **300** (5625), 1560-1563.

629

630 Randerson, J. T., Field, C. B., Fung, I. Y., Tans, P. P., 1999: Increases in early season ecosystem
631 uptake explain recent changes in the seasonal cycle of atmospheric CO₂ at high northern
632 latitudes. *Geophysical Research Letters*, **26**(17), 2765-2768.

633

634 Rawlins, M. A., McDonald, K. C., Frohking, S., Lammers, R. B., Fahnestock, M., Kimball, J. S.,
635 Vörösmarty, C. J., 2005: Remote sensing of snow thaw at the pan-Arctic scale using the
636 SeaWinds scatterometer. *Journal of Hydrology*, **312**(1), 294-311.

637

638 Rawlins, M. A., Nicolsky, D. J., McDonald, K. C., Romanovsky, V. E., 2013: Simulating soil
639 freeze/thaw dynamics with an improved pan-Arctic water balance model, *Journal of Advances in*
640 *Modeling Earth Systems*, **5**, 1-17

641

642 Reichle, R. H., Bosilovich, M. G., Crow, W. T., Koster, R. D., Kumar, S. V., Mahanama, S. P.,
643 Zaitchik, B. F., 2009: Recent advances in land data assimilation at the NASA Global Modeling
644 and Assimilation Office. *In Data Assimilation for Atmospheric, Oceanic and Hydrologic*
645 *Applications*, Springer Berlin Heidelberg, 407-428.

646 Reichle, R. H., Koster, R. D., De Lannoy, G. J., Forman, B. A., Liu, Q., Mahanama, S. P., Touré,
647 A., 2011: Assessment and enhancement of MERRA land surface hydrology estimates. *Journal of*
648 *climate*, **24**(24), 6322-6338.

649

650 Reichle, R. H., 2012: The MERRA-Land Data Product (Version 1.2). GMAO Office Note No. 3.
651 National Aeronautics and Space Administration (NASA). Available at
652 https://gmao.gsfc.nasa.gov/pubs/office_notes

653

654 Reichle, R. H., De Lannoy, G. J. M., Forman, B. A., Draper, C. S., and Liu, Q., 2014:
655 Connecting Satellite Observations with Water Cycle Variables through Land Data Assimilation:
656 Examples Using the NASA GEOS-5 LDAS. *Surveys in Geophysics*, in press

657

658 Rienecker, M. M., et al., 2011: MERRA: NASA's modern-era retrospective analysis for research
659 and applications. *Journal of Climate*, **24** (14), 624-3648.

660

661 Rignot, E., Echelmeyer, K., Krabill, W., 2001: Penetration depth of interferometric
662 synthetic- aperture radar signals in snow and ice. *Geophysical Research Letters*, **28**(18), 3501-
663 3504.

664

665 Rodell, M., Houser, P. R. , a1 Jambor, U. E., Gottschalck , J., K., Mitchell, C. J., Meng,
666 Arsenault, K., et al., 2004: The global land data assimilation system." Bulletin of the American
667 Meteorological Society **85** (3), 381-394.
668
669 Smith, N. V. Saatchi, S. S., and Randerson, J. T., 2004: Trends in high northern latitude soil
670 freeze and thaw cycles from 1988 to 2002. *Journal of Geophysical Research: Atmospheres* **109**
671 (D12)
672
673 Zhang, T., Armstrong, R. L., 2001: Soil freeze/thaw cycles over snow- free land detected by
674 passive microwave remote sensing. *Geophysical Research Letters*, **28**(5), 763-766.
675
676 Zhao, T., Zhang, L., Jiang, L., Zhao, S., Chai, L., Jin, R., 2011: A new soil freeze/thaw
677 discriminant algorithm using AMSR- E passive microwave imagery. *Hydrological*
678 *Processes*, **25**(11), 1704-1716.
679
680 Zuerndorfer, B., England, A. W., 1992: Radio brightness decision criteria for freeze/thaw
681 boundaries. *IEEE Trans Geosci Remote Sens.*, **30**(1), 89-102.
682
683
684
685
686
687

688

689

690

691

692 Table 1. Metrics for OL vs. truth estimates for a period of 8 years (2002-2010) and at 6am and

693 6pm local time. The RMSE for T_{surf} and T_{air} is computed excluding times and locations where

694 $T_{air} > 7^{\circ}\text{C}$ or $T_{air} < -7^{\circ}\text{C}$.

695

Variables	Metric	Value
T_{surf}	RMSE	3.08 °C
T_{soil}	RMSE	1.97 °C
F/T	Classification error	4.85%

696

697

698

699 Table 2. RMSE improvement ($\Delta RMSE = RMSE OL - RMSE DA$, in $^{\circ}C$) for T_{surf} and T_{soil} for
700 different maximum classification errors (CE_{max}), excluding times and locations where $T_{air} > 7^{\circ}C$
701 or $T_{air} < -7^{\circ}C$, for a period of 8 years (2002-2010) and at 6am and 6pm local time.

702

CE_{max} (%)	0%	5%	10%	20%
$\Delta RMSE$ ($^{\circ}C$)				
T_{surf}	0.206	0.192	0.178	0.149
T_{soil}	0.061	0.049	0.036	0.006

703

704

705

706

707

708

709

710

711

712

713

714

715

716 **Figure captions**

717 Figure 1. Schematic representation of the model diagnosis of the land surface F/T state as a
718 function of (snow-free) effective temperature (T_{eff}) and the snow cover fraction ($asnow$).

719

720 Figure 2. Schematic representation of three distinct F/T state regimes defined by upper and lower
721 uncertainty bounds on the effective temperature and snow cover thresholds for the purpose of the
722 F/T analysis. The upper bound for the snow cover threshold is set to $UB_{asnow}=100\%$.

723

724 Figure 3. Map of study domain.

725

726 Figure 4. Classification error function.

727

728 Figure 5. $\Delta RMSE$ (= $RMSE_{OL} - RMSE_{DA}$) in (a, c, e) T_{surf} and (b, d, f) T_{soil} across the study
729 domain for assimilation of synthetic F/T observations with (a, b) $CE_{max}=0\%$, (c, d) $CE_{max}=5\%$,
730 and (e, f) $CE_{max}=20\%$. A positive $\Delta RMSE$ indicates a skill improvement in the assimilation
731 results.

732

733 Figure 6. Spatially averaged $\Delta RMSE$ for (a,c,e) T_{surf} and (b,d,f) T_{soil} with 1 spatial standard
734 deviation around the mean as a function of the number of analysis updates for the assimilation of
735 synthetic F/T observations with (a,b) $CE_{max}=0\%$, (c,d) $CE_{max}=5\%$, and (e,f) $CE_{max}=20\%$. A
736 positive $\Delta RMSE$ indicates a skill improvement in the assimilation results.

737

738

739 Figure 7. Δ RMSE for (a) T_{surf} and (b) T_{soil} , as a function of the α parameter chosen in the

740 observation operator. A positive Δ RMSE indicates a skill improvement in the assimilation results.

741

742

743

744

745

746

747

748

749

750

751

752

753

754

755

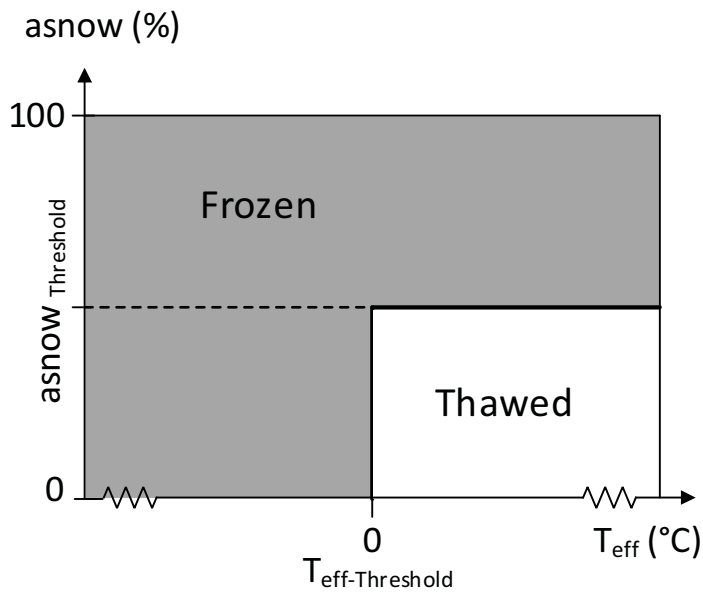
756

757

758

759

760



761

762 Figure 1. Schematic representation of the model diagnosis of the land surface F/T state as a

763 function of (snow-free) effective temperature (T_{eff}) and the snow cover fraction (*asnow*).

764

765

766

767

768

769

770

771

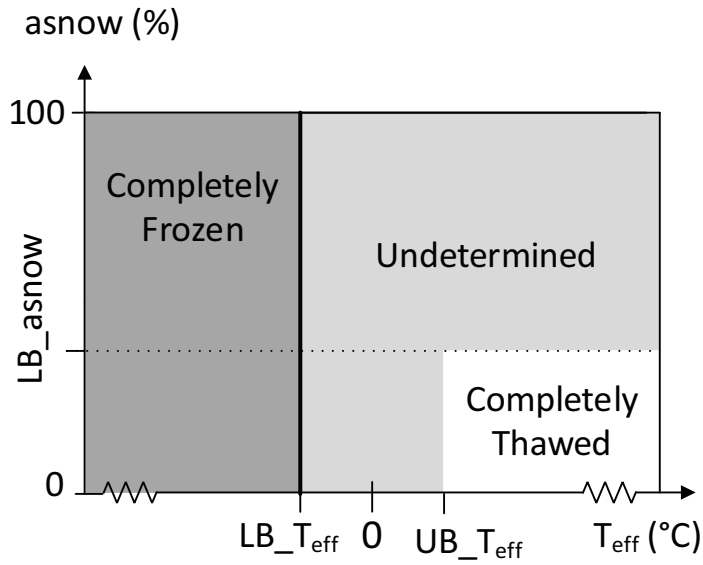
772

773

774

775

776



777

778 Figure 2. Schematic representation of three distinct F/T state regimes defined by upper and lower
779 uncertainty bounds on the effective temperature and snow cover thresholds for the purpose of the
780 F/T analysis. The upper bound for the snow cover threshold is set to $UB_{asnow}=100\%$.

781

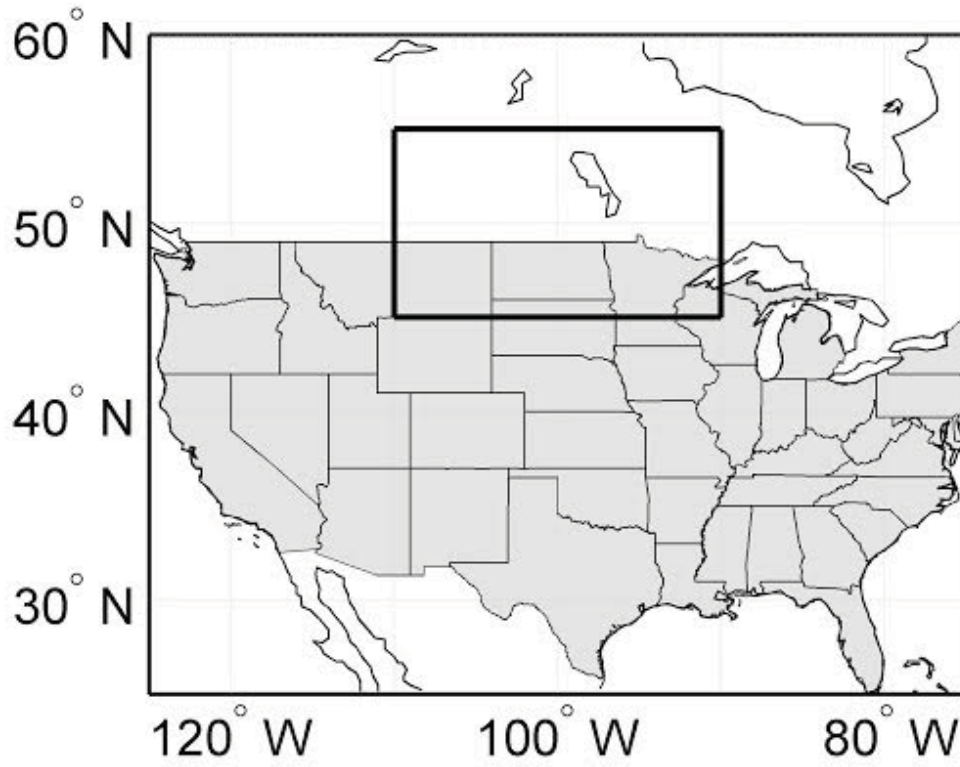
782

783

784

785

786



787

788 Figure 3. Map of study domain.

789

790

791

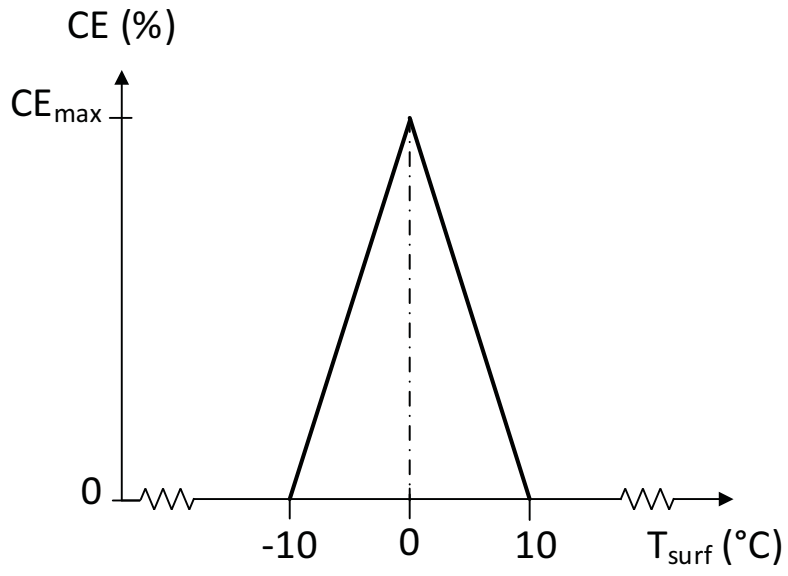
792

793

794

795

796

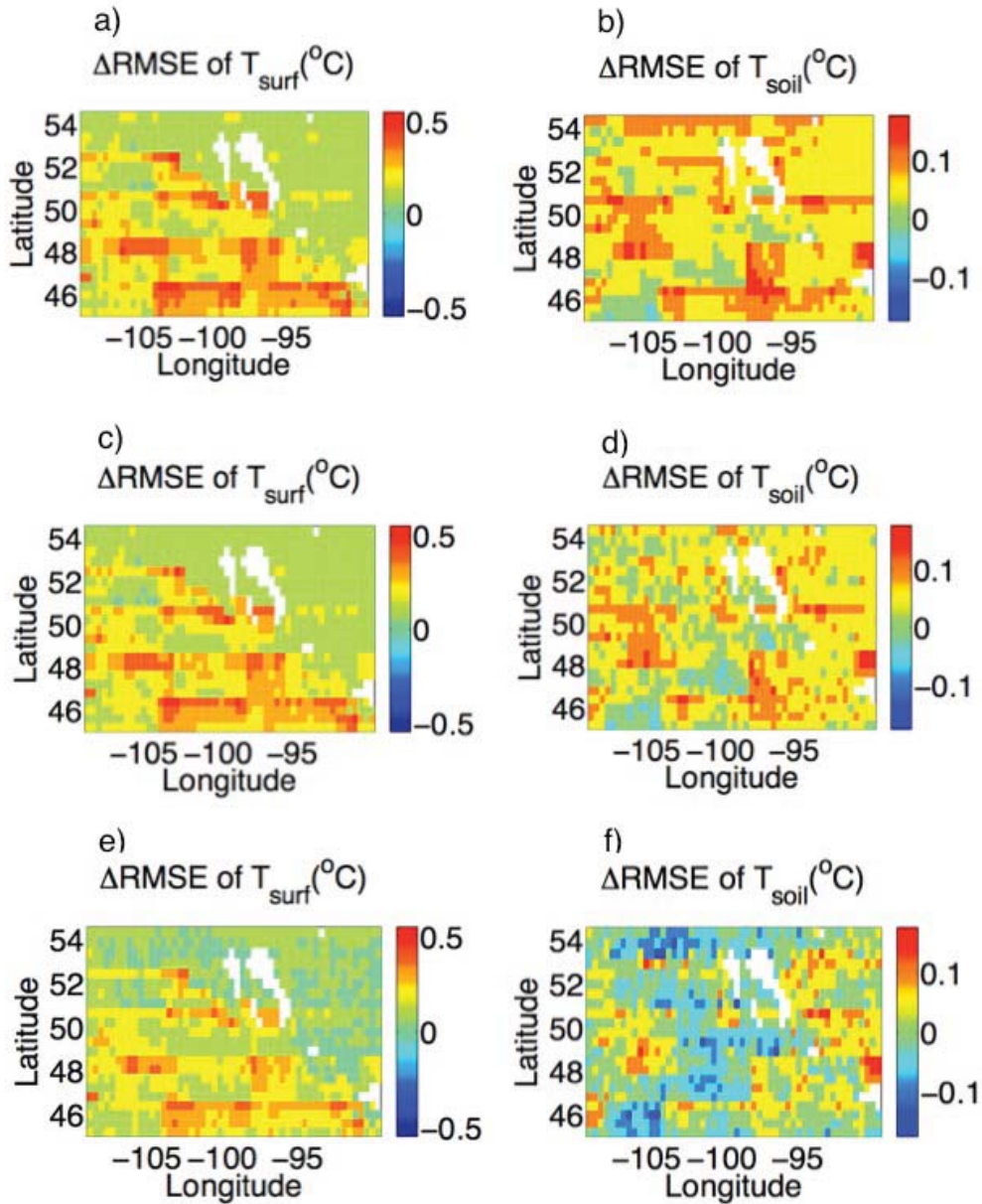


797

798 Figure 4. Classification error function.

799

800

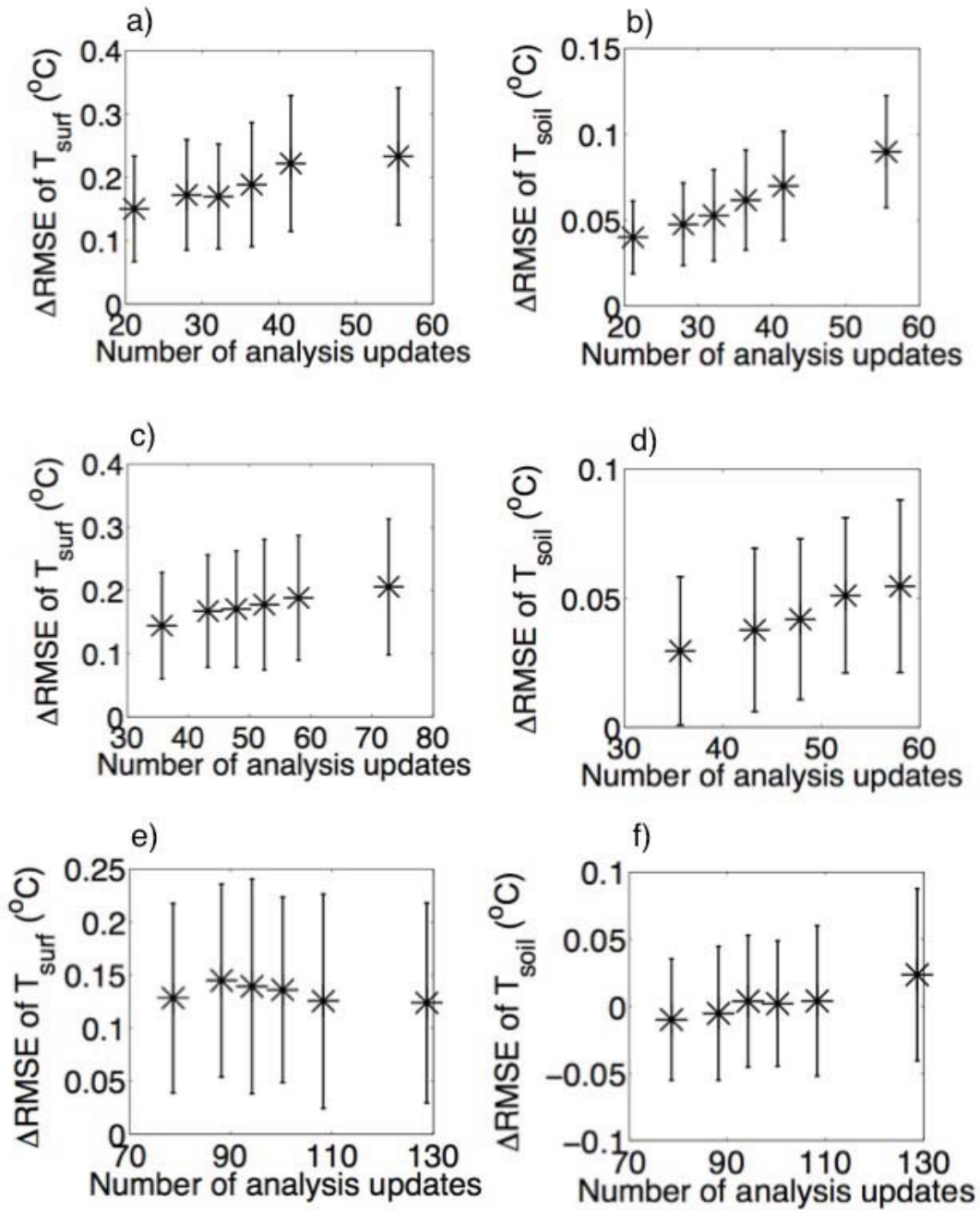


802

803 Figure 5. $\Delta RMSE$ (= $RMSE_{OL} - RMSE_{DA}$) in (a, c, e) T_{surf} and (b, d, f) T_{soil} across the study804 domain for assimilation of synthetic F/T observations with (a, b) $CE_{max}=0\%$, (c, d) $CE_{max}=5\%$,

805 and (e, f) $CE_{max}=20\%$. A positive $\Delta RMSE$ indicates a skill improvement in the assimilation
 806 results.

807
 808

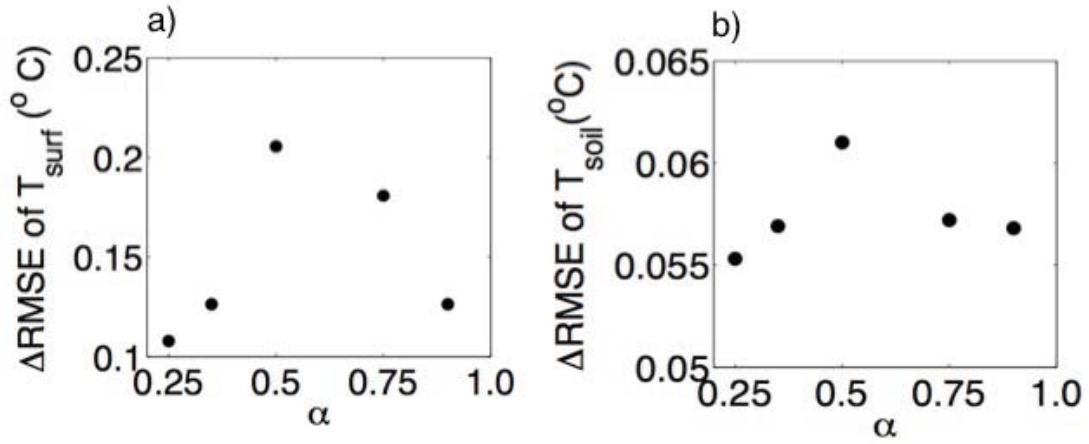


809

810 Figure 6. Spatially averaged $\Delta RMSE$ for (a,c,e) T_{surf} and (b,d,f) T_{soil} with 1 spatial standard

811 deviation around the mean as a function of the number of analysis updates for the assimilation of

812 synthetic F/T observations with (a,b) $CE_{max}=0\%$, (c,d) $CE_{max}=5\%$, and (e,f) $CE_{max}=20\%$. A
813 positive $\Delta RMSE$ indicates a skill improvement in the assimilation results.



814

815 Figure 7. $\Delta RMSE$ for (a) T_{surf} and (b) T_{soil} , as a function of the α parameter chosen in the
816 observation operator. A positive $\Delta RMSE$ indicates a skill improvement in the assimilation results.

817

818

819

820

821

822

823

824

825

826

827

828

829

830